JOURNAL OF MATERIALS SCIENCE 27 (1992) 4089–4096

Solution effect on the slow crack growth resistance of dilute sialons at high temperatures

I. TANAKA, G. PEZZOTTI, T. OKAMOTO, K. NIIHARA
The Institute of Scientific and Industrial Research, Osaka University, Mihogaoka 8-1, Ibaraki, Osaka 567, Japan

High purity Si_3N_4 powder was sintered with only 0.5–1.0 wt% AlN by hot isostatic pressing (HIP) and its delayed failure behaviour at around 1400 °C has been studied with interest to determine the role of Al atoms. Al atoms are found completely dissolved in the Si_3N_4 matrix as dilute sialon solid solutions by detailed analyses of phase composition. Flaw sensitivity increased considerably with the AlN addition, which was ascribed to the decrease in slow crack growth (SCG) resistance. Static-load lifetime under the same stress was remarkably decreased by the addition, which showed good agreement with that predicted from the experimentally obtained SCG resistance. Internal friction behaviour as well as microstructural investigation found no intergranular mechanisms for the SCG enhancement. Solution effect of Al and O atoms in the β-Si_3N_4 matrix and resulting virtual defect of covalent bonding was proposed to be their origin.

1. Introduction

Silicon nitride based ceramics are one of the most promising materials for structural applications at high temperatures, such as gas-turbine engines. Usually the aid of oxide additives for 5 to 20 volume % is necessary for their densification by liquid phase sintering process. The liquid remains as glassy or secondary-crystalline phases after the sintering and the nature of these intergranular phases often determine the high temperature properties of the sintered materials. Engineering of these phases has been, therefore, considered as the most important process for the design of Si_3N_4 materials [1, 2].

On the other hand, little attention has been paid to the qualities of the matrix Si_3N_4 grains. Especially when the interaction between crystalline defects and solute atoms is strong, solution effects must be significant, as is often the case in metallic alloys. Some solute atoms may modify the electronic structure behind the mechanical properties of the matrix material considerably. But, few works have explicitly examined these effects in Si_3N_4, so far, probably because of the lack of a pure Si_3N_4 material which can be used as a reference material for such investigations. As shown in our previous reports [3–6], high purity Si_3N_4 powder can be fully densified without additives by hot isostatic pressing, and the sintered body shows superior delayed failure resistance up to 1400 °C compared with other Si_3N_4 materials sintered with various kinds of additives. Its composition and microstructures are very simple: it can, therefore, be considered as a reference material for sintered Si_3N_4.

In the present study, influences of Al-addition on high temperature mechanical properties have been pursued, because Al and O can be double-substituted to Si and N in β-Si_3N_4 and form β-sialon solid solution [7, 8]. It is also important, because Al_2O_3 and AlN are often used as sintering aids for Si_3N_4. The Si_3N_4 powder containing SiO_2 impurity of 2.4 wt % was mixed with 0.5 to 1.0 wt % of an AlN powder, and the solid solutions were made through reaction between AlN, Si_3N_4 and SiO_2. The effect of Al_2O_3 addition for the same Al concentration was also examined for comparison. After studying the phase composition and microstructures, effects of Al and O atoms on slow crack growth (SCG) behaviour at high temperatures were carefully evaluated and their roles were discussed from the atomistic point of view.

2. Experimental procedure

2.1. Sample preparation

Commercial high purity Si_3N_4 powder (E10, Ube) used throughout the present work was identical to that used in our previous studies [3–6]. It contains oxygen, 1.3 wt % (SiO_2: 2.4 wt %) and less than 100 wt p.p.m. of other impurities. Detailed impurity contents obtained by inductively-coupled radio-frequency plasma emission spectrometer (ICP) were shown in a previous report [4]. An AlN powder (Type F, Tokuyama-Soda) containing oxygen 0.9 wt% and cation impurities < 100 wt p.p.m. was mixed with the Si_3N_4 powder, 0.5 and 1.0 wt %, corresponding to

0.33 and 0.66 wt % of Al concentration. For comparison, aluminium isopropoxide, $Al(OC_3H_7)_3$, (Nakarai) was dissolved in ethanol and mixed with the Si_3N_4 powder, 0.66 wt % of Al concentration (corresponding to Al_2O_3 of 1.24 wt %). Fine Al_2O_3 particles were reported to be obtained after calcination of $Al(OC_3H_7)_3$ [9]. The mixed powder was milled for 24 h in a polypropylene jar with SiC balls in ethanol, and then dried at 140 °C for 10 h. Samples were preformed by cold isostatic pressing (CIP) at 200 MPa to 50% of theoretical density, and then coated by BN powder (UHP–FM, Showa Denko) by CIP again at 200 MPa. The green compacts were pre-fired *in vacuo* of 10^{-3} Pa at 1200 °C and then encapsulated into borosilicate glass tube (Pyrex, Corning). Sintering was carried out by hot isostatic pressing (HIP) for 2 h operated at 1950 °C with 170 MPa of Ar gas pressure. Density after the sintering measured by water displacement method was $> 3.18\ g\ cm^{-3}$ which corresponds to more than 99.5% of theoretical density of Si_3N_4.

Crystalline phases were identified, after crushing the specimens, by powder X-ray diffractometry with CuK_α radiation. Only β-Si_3N_4 was detected in all specimens, neither α-Si_3N_4 nor Si_2N_2O was detected. Lattice constants of the β-Si_3N_4 were determined by least-square fitting using Si powder as an internal standard.

2.2. Microstructural observations

The microstructure of the sintered bodies was examined by scanning electron microscopy (SEM) in lapped surfaces after etching in molten NaOH at 380 °C for 1 min. Observation of grain boundary phase was performed by transmission electron microscopy (TEM) with a field-emission type electron gun (H600FE, Hitachi) operated at 100 kV. Energy dispersive X-ray spectroscopy (EDX) and electron energy loss spectroscopy (EELS) were used for microanalyses. Specimens for the observation were prepared by diamond cutting, grinding and polishing to form thin slices of 50 μm, and ion-thinning. They were then coated by evaporated carbon for about 5 nm to suppress surface charging.

2.3. Mechanical tests

Flexural strength was measured for specimens of $3 \times 4 \times 40\ mm^3$ up to 1400 °C in air by a 4-point bending test with a universal testing machine (1185, Instron). The surface of the specimen was ground with a 600 grit diamond wheel and their edges were removed carefully for 0.1 mm. The inner and outer spans were 30 and 10 mm, respectively.

SCG resistance proposed in a previous study [5] was evaluated by stepwise-loading of indentation-precracked specimens. A controlled surface flaw was introduced by a Vickers indentation of 49 N at the centre of the tensile surface of bending bars. Specimens were annealed for 1 h at above 1200 °C in order to release the residual stress introduced by the indentation. Specimens were loaded stepwisely (10 MPa/10 min) in three point bending geometry with a span of 15 mm until failure. Constant load was applied by a load-cycling method in the testing machine. Scattering of the load was within 2% of the applied load. Fracture surface after the test was observed by optical microscopy to measure the initial and final flaw sizes, and fracture mode was examined by SEM. SCG resistance and apparent fast fracture resistance (fracture toughness) were calculated using

$$K_I^* = Y_0 \sigma_{final} a_0^{1/2} \quad (1)$$

$$K_R^{ap} = Y_{final} \sigma_{final} a_{final}^{1/2} \quad (2)$$

where Y, σ and a are geometric factor, applied stress and flow size, and subscripts 0 and final refer to the initial flaw and final stress at the fracture, respectively.

SCG rate is usually expressed by nth power of stress intensity as

$$da/dt = AK_I^n \quad (3)$$

The time to failure, t_f, under the SCG condition is given by integrating Equation 3 as

$$t_f = 2/(n-2)A^{-1} Y^{-n} a_0^{(2-n)/2} / \langle \sigma^n \rangle \quad (4)$$

in which A is a constant and $\langle \sigma^n \rangle$ shows the average of nth power of applied stress, σ^n, that is

$$\langle \sigma^n \rangle = 1/t_f \int_0^{t_f} \sigma(t')^n dt' \quad (5)$$

The term $a_{final}^{(2-n)/2}$ was neglected because it is much smaller than the term $a_0^{(2-n)/2}$ when n-value is larger than 10, as often observed for SCG behaviour of engineering ceramics, at high temperatures.

Lifetime under static load (t_s) of σ_{final} for the specimen with initial flaw of a_0 is given by Equation 4 as

$$t_s = 2/(n-2)A^{-1} Y^{-n} a_0^{(2-n)/2} / \sigma_{final}^n \quad (6)$$

From Equations 4 and 6, the meaning of SCG resistance as defined in Equation 1 can be given. It is an initial stress intensity corresponding to an effective static-load lifetime of

$$t_s = \langle \sigma^n \rangle / \sigma_{final}^n t_f \quad (7)$$

In the stepwise loading tests, t_s is given by

$$t_s = t_f / N \sum_{j=1}^{N} \sigma_j^n / \sigma_{final}^n \quad (8)$$

where t_f is total loading time and N is the number of stress-steps during the test. Stepwise load of 10 MPa/10 min was applied to specimens, and t_s was approximately 10^3 s.

Internal friction was measured at frequency of 12 Hz from 25–1350 °C in nitrogen gas of 50 kPa by an inverted torsion pendulum apparatus which was reported elsewhere [10]. All the measurements were automatically made on both heating and cooling runs each at 3 °C.

3. Results

3.1. Phase composition

Sintered bodies were subjected to ICP analysis and no impurity contamination during the processing was

TABLE I Nominal composition, results of chemical analysis and powder X-ray diffraction for 0 and 1.0 wt % AlN materials

Nominal			Chemical analysis	X-ray		
AlN addition (wt %)	Al (wt %)	z	Al (wt %)	a (0.1 nm)	c (0.1 nm)	z
0	0	0	< 0.003	7.601	2.907	0
1.0	0.66	0.069	0.64	7.603	2.909	0.07

found. This is similar to the findings of a previous study [4]. The general form of β-sialons is usually given as $Si_{6-z}Al_zO_zN_{8-z}$ [7]. The z value calculated from the Al content was shown together.

Lattice parameters of β-Si_3N_4 were determined by powder X-ray diffractometry as shown in Table I. In Si_3N_4 sintered without additives, they were determined to be $a = 0.7601$ nm and $c = 0.2907$ nm, which are close to those reported by Ekström and Olsson [11] by extrapolation of β-sialon series in the range of $0.25 < z < 3.8$. Although the increments were very small, both a and c were found to increase with the Al content systematically. Assuming the linear relationships between the z-value and the lattice parameters given by Ekström and Olsson [11], z-values for the present samples can be estimated as listed in Table I.

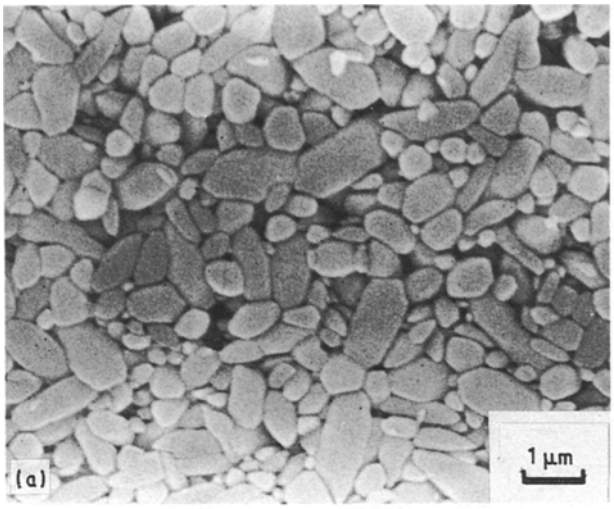

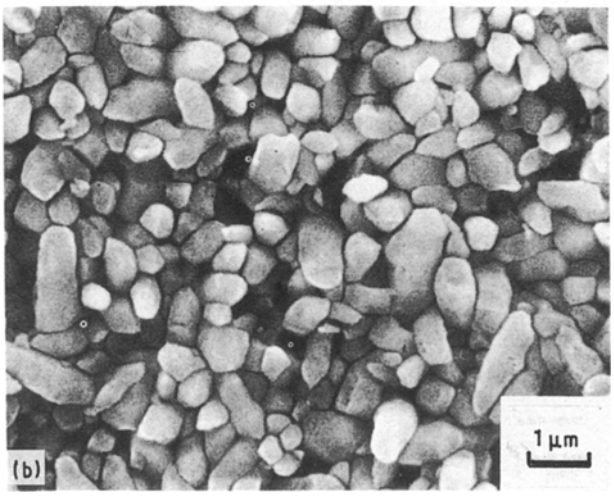

Figure 1 Scanning electron micrographs of sintered bodies: (a) Si_3N_4 without additives; and (b) Si_3N_4–1.0 wt % AlN material.

They showed fairly good agreement with those estimated from the chemical analysis.

3.2. Microstructures

Fig. 1 shows the SEM of sintered bodies with and without an addition of 1.0 wt % of AlN. As can be seen, their mean grain size and grain morphology are almost the same. No significant grain elongation can be observed in both materials. Transmission electron micrographs of typical grain boundaries are presented in Fig. 2. Existence of glassy silica at the grain boundary triple point was identified by nano-beam electron diffraction with a minimum probe diameter of 5 nm, and microanalyses by EDX and EELS. No enrichment of Al atoms at grain boundary phase was detected by EDX. Moreover, Al content was measured by EDX in more than 20 grains with a small probe-size (50 nm) and the result was not different (within experimental error) to the total Al concentration obtained with a large probe-size (10 μm).

It can be concluded that large amounts of Al atoms dissolved into the β-Si_3N_4 phase, as expected from the chemical analysis data and X-ray diffraction results (Table I). Contents of glassy SiO_2 decreased during the formation reaction of the sialon solid solution. As a result, the average size of the glassy phase at the triple point was smaller in the AlN-added sample. But, the width of the grain boundary film between two grains seems unchanged by the addition of AlN.

Fracture toughness of Si_3N_4–1 wt % AlN material was 4.0 MPa $m^{1/2}$ by the indentation microfracture method [12] which was about 30% larger than that of Si_3N_4 sintered without additives [3].

3.3. High temperature strength and flaw severity

Flexural strength measured at an outer fibre strain rate of 1.5×10^{-4} s^{-1} (crosshead speed of 0.5 mm min^{-1}) of 1.0 wt %–AlN material and Si_3N_4 without additives as a function of temperature are plotted in Fig. 3. No strength degradation was observed in both specimens up to 1400 °C at this strain rate. But with the increase of AlN addition, flaw severity of specimens found to decrease at 1400 °C. Fig. 4 shows the bending strength at 1400 °C for as-machined and indentation flawed (Vickers 5 kg at room temperature) specimens as a function of AlN addition. Radii of semicircular flaws introduced by the indentations were 130, 120 and 115 μm for 0, 0.5 and 1.0 wt % AlN materials, respectively. Significant intergranular SCG was only apparent in fractographs of

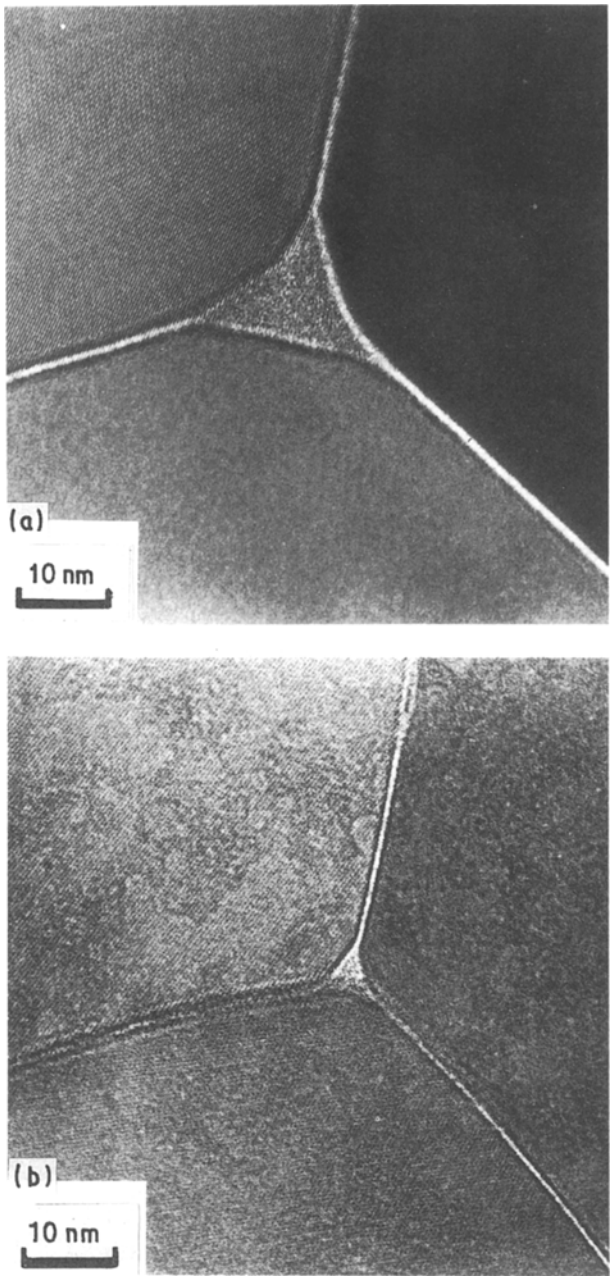

Figure 2 Transmission electron micrographs of intergranular phase in: (a) Si_3N_4 without additives; and (b) Si_3N_4–1.0 wt % AlN material.

AlN-added and indented specimens as can be seen in Fig. 5. In order to observe the SCG profiles, several Vickers-indentations (5 kg) were made on lapped tensile surface of 1.0 wt %–AlN specimens: constant stress of 140 MPa was applied to the specimen by a 4-point bending geometry at 1400 °C until fracture, which occurred at one of the indentation-induced flaws at the SCG–fracture origin. SCG profiles were observed at other indentation-induced flaws which suffered SCG but did not propagate until failure. SCG propagated intergranularly, contrary to the transgranular crack propagation at room temperature in the same material as can be seen in Fig. 6. Neither creep damage nor plastic strain were found in all specimens. The strength degradation in AlN-added materials is most likely ascribed to the decrease in SCG resistance, which will be hereafter discussed in detail.

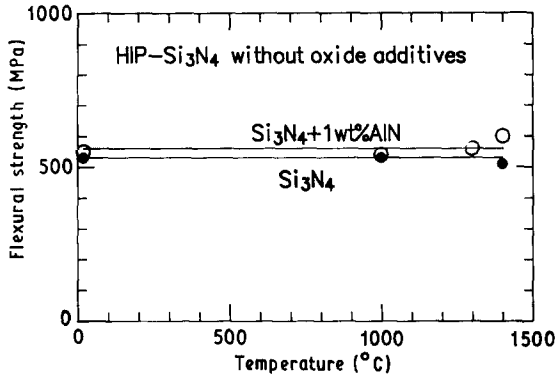

Figure 3 Flexural strength as a function of temperature, $\dot{\varepsilon} = 1.5 \times 10^{-4}\,s^{-1}$.

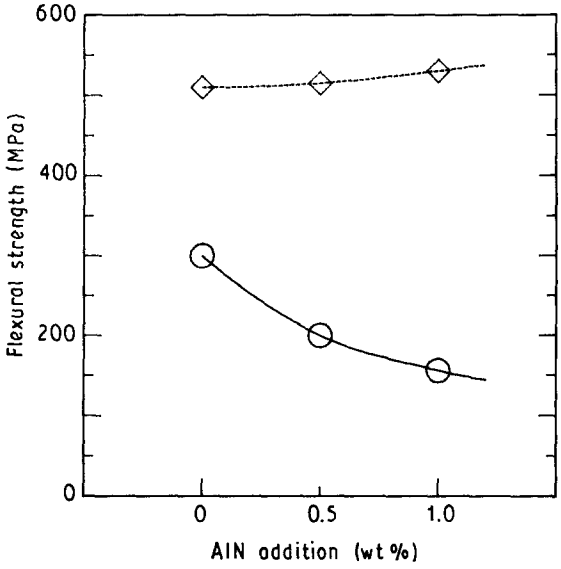

Figure 4 Flexural strength at 1400 °C as a function of AlN addition: (◇) as-machined; (○) Vickers = 5 kg, $\dot{\varepsilon} = 1.5 \times 10^{-4}\,s^{-1}$.

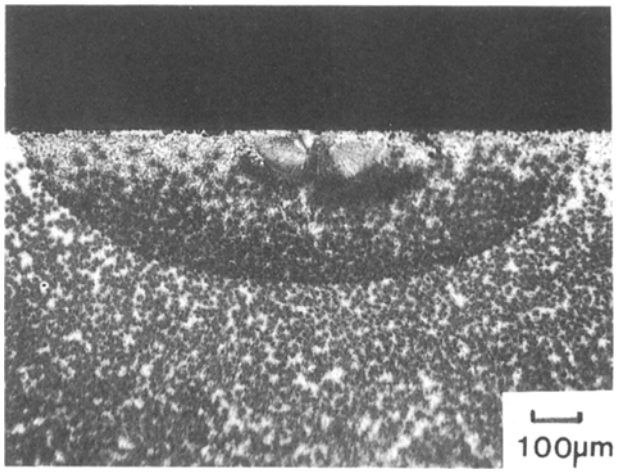

Figure 5 Fractograph of 1.0 wt % AlN specimen subjected to bending test with strain rate of $1.5 \times 10^{-4}\,s^{-1}$. Vickers indentation of 5 kg was made prior to the test.

In order to measure the SCG resistance quantitatively in static-loading condition, indentation-flawed (Vickers 5 kg) specimens were loaded step-wisely until fracture. Applied load as a function of time is shown in

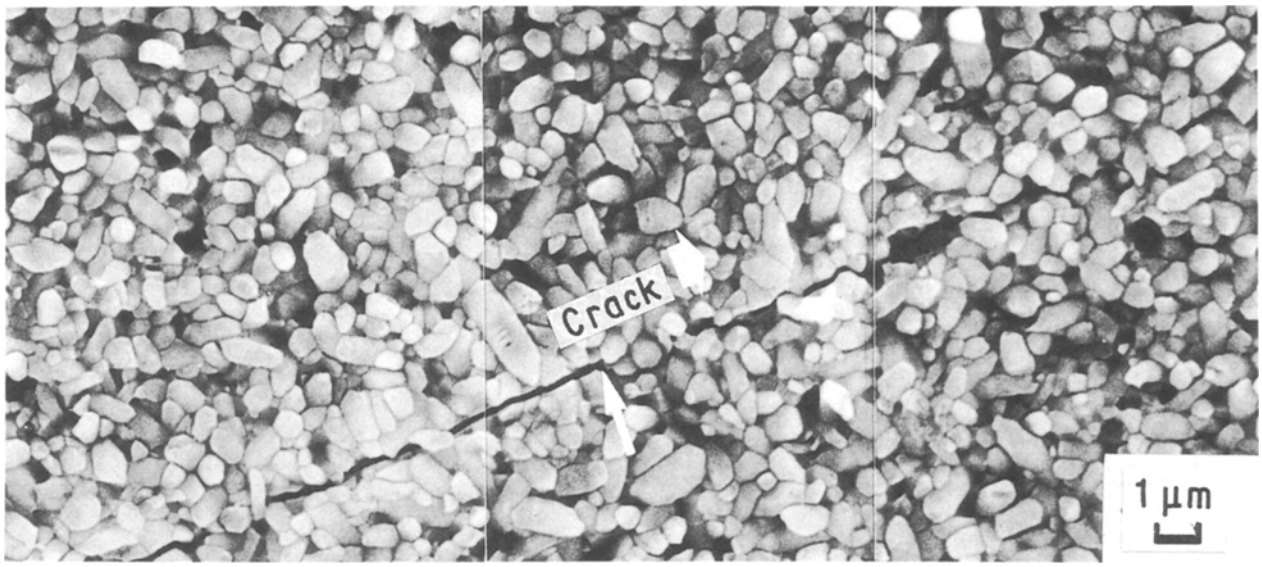

Figure 6 Crack profile of indentation-induced flaw (left, straight) and SCG (right). The starting point of SCG is indicated by a white arrow.

Fig. 7, and the failure stresses are indicated by arrows. The SCG resistance and apparent fast-fracture resistance were calculated with Equations 1 and 2 using fracture stress and initial/final crack length measured at fracture surface. The SCG resistance means the initial stress intensity corresponding to the effective static-loading lifetime, t_s given by Equation 8. In the present experimental conditions, t_s was about 10^3 s and only weakly dependent on the n-value. The SCG resistance as a function of temperature is plotted in Fig. 8. In the 1.0 wt %–AlN material, SCG resistance started to decrease remarkably at above 1300 °C. Apparent fast-fracture resistance was shown in Fig. 9 as a function of temperature. In both materials, it gradually increased above 1300 °C. But, the difference between 0 and 1.0 wt % AlN materials was not significantly changed from that at room temperature. The increase may be simply ascribed to the energy dissipation phenomena due to decrease of grain boundary viscosity. Degradation of SCG resistance and increase of apparent fracture toughness at 1400 °C was also found in 1.24 wt % Al_2O_3-added specimen (Al: 0.66 wt %). These values obtained by the step-wise-loading test of Vickers indented specimens are shown together in Figs 8 and 9.

Lifetime under static-load was measured to confirm the above-mentioned SCG resistance data. It was measured in as-machined bending-specimens at 1400 °C and shown in Fig. 10. As can be seen, the lifetime in 1.0 wt %AlN material was found about 4 orders of magnitude smaller than that in 0 wt %AlN compared at the same stress level. The data will be compared with the SCG resistance data in the following section.

Internal friction of 1.0 wt %–AlN specimen was measured by torsion pendulum method up to 1350 °C at frequency of 12 Hz. The result was shown in Fig. 11 together with that measured for Si_3N_4 without additives. Only high temperature background increases were observed in both of the materials. The apparent

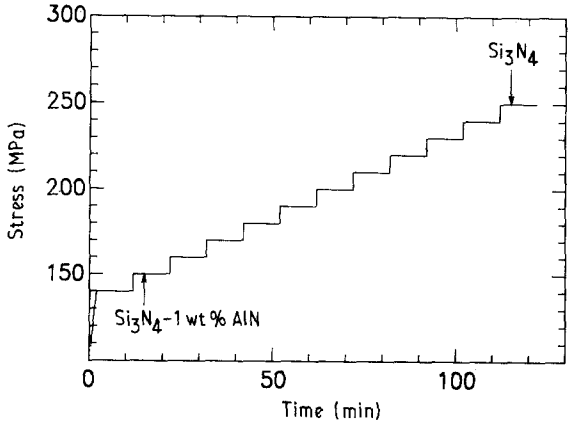

Figure 7 Schedule of the step-wise loading test (10 MPa/10 min). Failure points when tested at 1400 °C in air are indicated by arrows, initial flaw-Vickers = 5 kg.

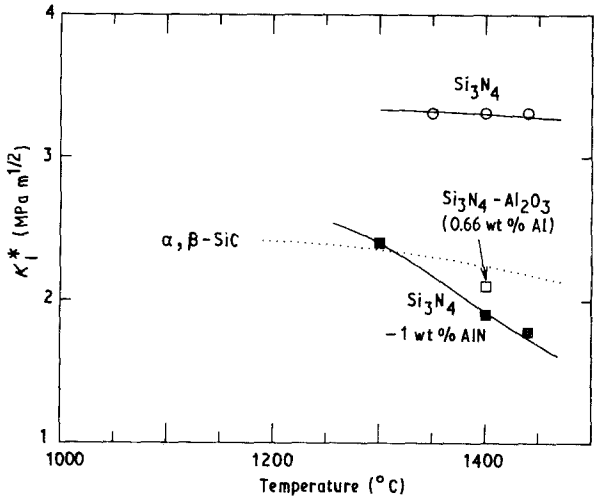

Figure 8 SCG resistance ($t_s \sim 10^3$ s) experimentally obtained as a function of temperature. Data of α and β-SiC are shown for comparison [5].

fracture toughness shown in Fig. 9 starts to increase similarly to the background increase, indicating that their origins are the same; that is the softening of the intergranular glassy phase. The background intensity

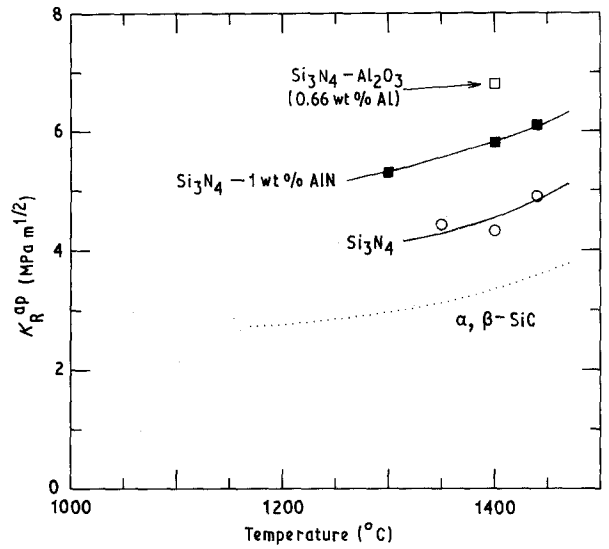

Figure 9 Apparent fast fracture resistance obtained as a function of temperature. Data for SiC's are from [5].

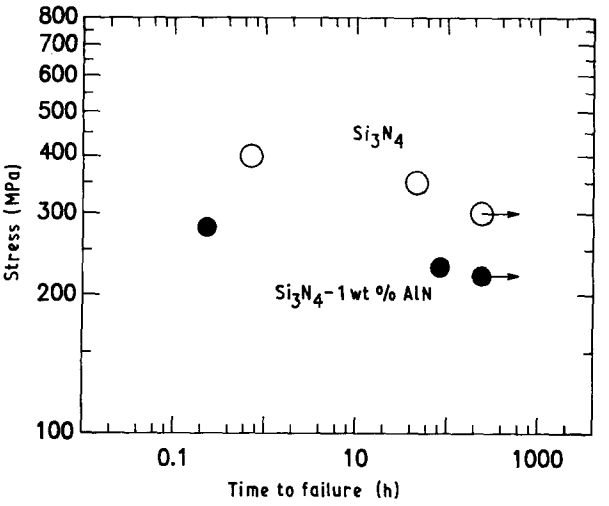

Figure 10 Lifetime measured at various static loads at 1400 °C. Tests were finished after 240 h, and an arrow indicates that the material was not broken within 240 h.

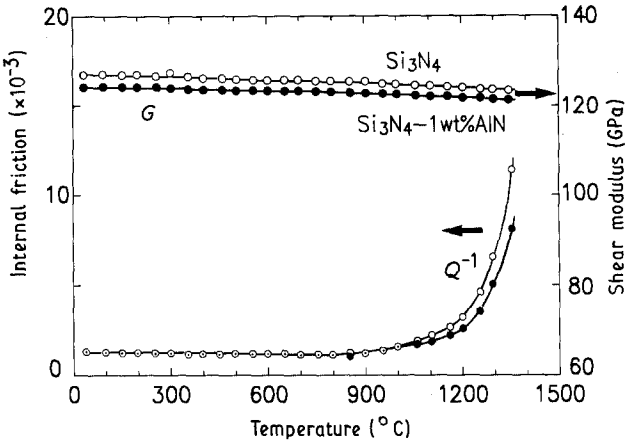

Figure 11 Internal friction (Q^{-1}) and shear modulus (G) measured as a function of temperature.

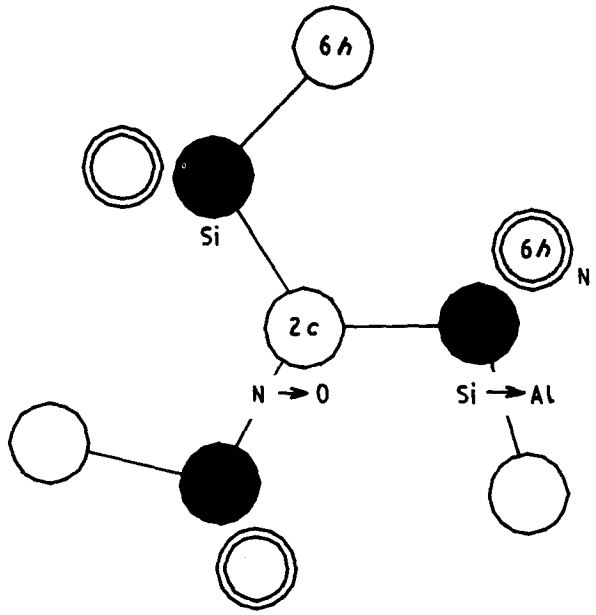

Figure 12 A part of basal plane projection of β-Si_3N_4 structure. Double open circles indicates the presence of two atoms at the same projected plane.

was smaller in the 1.0 wt %–AlN specimen, probably because volume fraction of glassy silica was decreased by the sialon formation with AlN and Si_3N_4 and the impurity SiO_2.

If some kinds of impurities, such as silica-glass modifiers, were localized in the intergranular glassy phase, a relaxation peak should be superposed on the background [4]: the peak has been ascribed to the impurity enhanced atomic jump in the glassy phase, which significantly promote the intergranular cavity formation rate at higher temperatures [4]. Such a peak was not found in AlN-added specimen indicating the absence of impurity-enhanced intergranular cavity formation mechanism.

4. Discussion

4.1. Solution effects for high temperature strength

The present experiments clearly showed that the SCG resistance decreases above 1300 °C when AlN or Al_2O_3 is added (as much as 0.6 wt % of Al concentration). The Al atoms were found almost dissolved in the Si_3N_4 matrix grains. Moreover, no significant difference in mechanical properties of the intergranular glassy phase was detected by the internal friction method. The dissolved Al atoms therefore may contribute to the high temperature strength degradation. Possible atomistic mechanism for the solution effect can be discussed as follows.

In a previous report [13], high purity β-sialon powders synthesized from the silicon di-imides were sintered without additives by a method identical to the present investigation. The sialon powders with z-values of 2 and 3 containing practically no excess oxides could be fully densified at around 1500–1700 °C which is about 250–450 °C lower than the temperature necessary to fully densify the high purity Si_3N_4 powder by the same sintering process. The fact suggests that the elementary processes of sintering, such as volume diffusion, grain boundary

diffusion and dislocation motion, are much faster when these solute atoms are present in the Si_3N_4 matrix because of the considerable solution effects.

X-ray diffraction analyses revealed that the crystal structure of β-sialon solid solution is identical to that of β-Si_3N_4 [7]. Neutron diffraction analyses [14] found no structural vacancies in the solid solution. Basal-plane projection of a. part of β-Si_3N_4 and β-sialon ($z = 2$) structures are shown in Fig. 12. A stick between two balls in the figure shows a bond between an anion and a cation. Solute oxygen atom may preferentially occupy the 2*c*-site (Wyckoff notation) according to the neutron diffraction results. The solute Al atom most probably occupies the nearest neighbour cation position of the 2*c* oxygen site to maintain the charge neutrality. When these solute atoms sit on these positions, covalent bonding around the oxygen atom may be significantly weakened. The solution of Al–O pair may act as the centre of virtual defect of chemical bonding. Presence of such a bonding-defect may play an important role for the enhancement of atomic diffusivity and dislocation mobility through the strong interaction between crystalline defects. Detailed calculations for the electronic structures can be found in a separate paper [15].

4.2. Lifetime prediction at 1400 °C under static-loading condition

In the region where SCG behaviour determines the lifetime or fracture stress, the SCG resistance data should be comparable to other experimentally obtainable parameters, such as static-load lifetime and bending strength measured by constant loading rate.

Lifetime, t_{sx} under constant stress of σ_{sx} when initial flaw geometry is expressed by geometric factor Y_{0x} and flaw size a_{0x} is given by

$$t_{sx} = a_{0x}/a_{0s}((Y_{0s}\sigma_{fs}a_{0s}^{1/2})^n/(Y_{0x}\sigma_{sx}a_{0x}^{1/2}))^n t_{ss} \quad (9)$$

where Y_{0s}, a_{0s}, σ_{fs} and t_{ss} are geometric factor, initial flaw size, failure stress and effective static-load lifetime in the step-wise loading test, respectively. Lifetime was calculated for $a_{0x} = 20\,\mu m$ and $40\,\mu m$ and $n = 20$ as a function of applied stress as shown in Fig. 13. As can be seen, the calculated lifetime showed fairly good agreement with the experimental values assuming that initial flaw size is ranging from 20–40 μm.

The effective static-load lifetime of bending test measured at constant loading rate is given by

$$t_{sd} = \sigma_{fd}/[\dot{\sigma}_d(n+1)] \quad (10)$$

where σ_{fd} and $\dot{\sigma}_d$ are fracture stress and stressing rate. σ_{fd} for the same initial flaw size as that of step-wise loading test can be given by

$$\sigma_{fd} = [\sigma_{fs}^n t_{ss}\dot{\sigma}_d(n+1)]^{(1/n+1)} \quad (11)$$

The fracture strength for different initial flaw size can be deduced from Equation 6. Fig. 14 shows the calculated strength at 1400 °C based on SCG resistance obtained from step-wise loading data. Initial flaw size was taken to be the same as the step-wise test (5 kg Vickers), 20 and 40 μm, n was assumed to be 20. As can be seen, the strength degradation behaviour with the increase of AlN addition in Vickers-indented specimens can be well reproduced by the calculation. The small difference in absolute values may arise from the error accumulation during fairly long extrapolation. Strength should not exceed the fast fracture level which is around 500–600 MPa in the present materials. By taking into account the truncation, dependence of strength in as-machined specimens on AlN addition can also be well simulated.

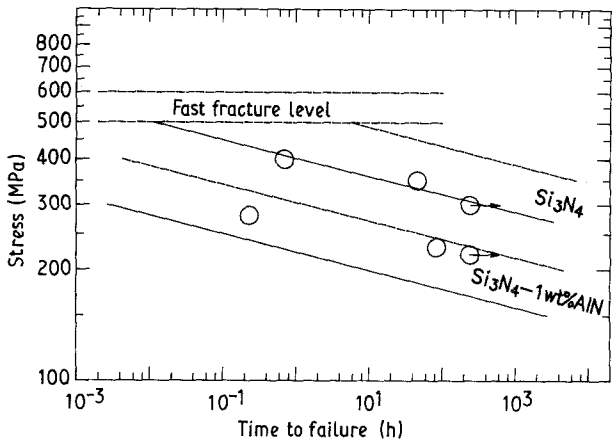

Figure 13 Results of the lifetime prediction at 1400 °C compared with the lifetime based on the present SCG resistance data: $n = 20$; initial flaw: (——) 40; (– – –) 20 μm.

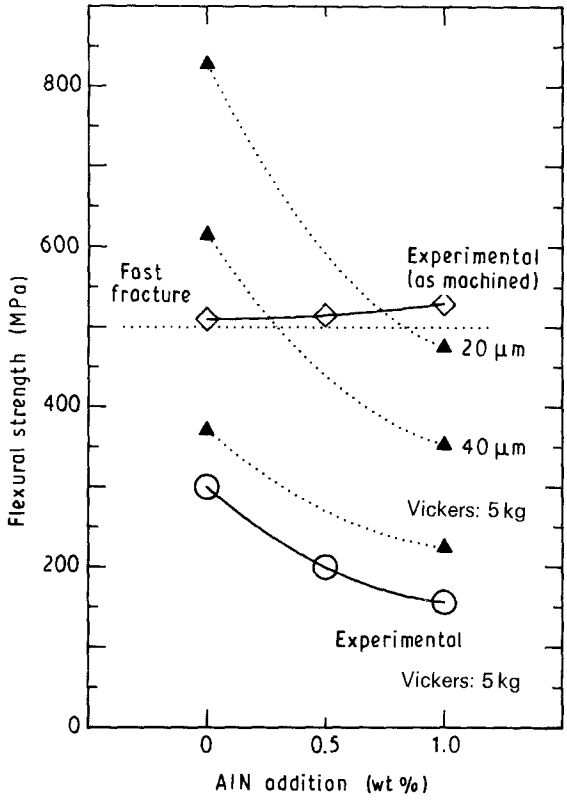

Figure 14 Bending strength calculated for as-machined and Vickers indented specimens. (▲) are data calculated with the SCG resistance data, at 1400 °C, $\dot{\varepsilon} = 1.5 \times 10^{-4}\,s^{-1}$ and $n = 20$.

5. Summary

Solution effect of Al and O for the high temperature delayed failure strength of β-Si_3N_4 sintered body has been demonstrated in the present systems. Al has been added to high purity Si_3N_4 either from AlN and Al_2O_3 0.3–0.6 wt %Al, and fully densified by hot isostatic pressing. Their SCG resistance decreased significantly above 1300 °C: lifetime under static-tensile loading at 1400 °C in the 1.0 wt %AlN material was about 4 orders of magnitude shorter than the case without additives, which showed good agreement with the value calculated from experimentally obtained SCG resistance. Flaw severity in the AlN-added materials was also well interpreted by the decrease of SCG resistance. The presence of virtual defect of covalent bonding was proposed as the origin of the solution effect.

Acknowledgements

The authors are sincerely grateful to Messrs A. Koreeda and T. Ishibashi of ISIR, Osaka University for their helps in TEM observation; and Messrs Y. Kohtoku and T. Nakayasu of Ube Corporation for impurity analyses.

References

1. R. N. KATZ and G. E. GAZZA in "Nitrogen Ceramics" edited by F. L. Riley (Noordhoff-Leyden, 1977) pp. 417–31.
2. G. ZIEGLER, J. HEINRICH and G. WOTTING, *J. Mater. Sci.* **22** (1987) 3041.
3. I. TANAKA, G. PEZZOTTI, T. OKAMOTO, Y. MIYAMOTO and M. KOIZUMI, *J. Amer. Ceram. Soc.* **72** (1989) 1656.
4. I. TANAKA, G. PEZZOTTI, K. MATSUSHITA, Y. MIYAMOTO and T. OKAMOTO, *ibid.* **74** (1991) 752
5. I. TANAKA and G. PEZZOTTI, *ibid.* submitted.
6. *Idem, ibid.* **75** (1992) in press
7. K. H. JACK, *J. Mater. Sci.* **11** (1976) 1135.
8. Y. OYAMA and O. KAMIGAITO, *Jpn J. Appl. Phys.* **10** (1971) 1637.
9. K. KISHI, S. UMEBAYASHI, E. TANI and K. KOBAYASHI, *J. Ceram. Soc. Jpn (Yogyo Kyokai-shi)* **92** (1984) 231.
10. K. MATSUSHITA, PhD Thesis, Osaka University (1990).
11. T. EKSTRÖM and P.-O. OLSSON, *J. Amer. Ceram. Soc.* **72** (1989) 1722.
12. K. NIIHARA, R. MORENA and D. P. HASSELMAN, *ibid.* **65** (1982) C116.
13. Y. FUJIWARA, I. TANAKA, S. KUME, T. OKAMOTO and Y. MIYAMOTO, *J. Ceram. Soc. Jpn, (Yogyo Kyokai-shi)* **98** (1990) 360.
14. F. K. VAN DIJEN, R. METSELAAR and R. B. HELMHOLDT, *J. Mater. Sci. Lett.* **6** (1987) 1101.
15. I. TANAKA, S. NASU, H. ADACHI, Y. MIYAMOTO and K. NIIHARA, *Acta Met. Mater.* (1992) in press.

Received 4 April
and accepted 30 July 1991